Engineering Structures 288 (2023) 116186

Contents lists available at ScienceDirect

Engineering Structures

journal homepage: www.elsevier.com/locate/engstruct

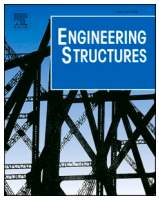

Development and seismic performance evaluation of New high strength reinforced concrete column and steel beam (New-RCS) joint

Yu-Chen Ou [a,*], Jones Joju [a], Bo-Cheng Lai [a], Jui-Chen Wang [b]

[a] Department of Civil Engineering, National Taiwan University, No. 1, Sec. 4, Roosevelt Road, Taipei 106, Republic of China
[b] Ruentex Engineering & Construction Co., Ltd., No. 308, Section 2, Bade Road, Taipei 106, Republic of China

ARTICLE INFO

Keywords:
RCS
Beam-column joint
High strength
Beam hinging
Joint bearing strength
Design code
Material overstrength
Cyclic test
Composite structures

ABSTRACT

Reinforced Concrete column and Steel beam (RCS) structural systems have recently become popular in Taiwan for office buildings. High seismic demand makes the size of conventional concrete columns enormous and the reinforcement over-crowded, which can be solved using high-strength materials. However, due to the lacuna of research regarding the usage of high-strength materials, existing design guidelines for the RCS systems have restricted the maximum grade of steel reinforcement to 410 MPa. Also, using high-strength materials in RCS joints necessitates innovative joint detailing and design to develop sufficient joint bearing and shear strength. Thus, a new high-strength reinforced concrete column and steel beam (New-RCS) joint was developed in this study, incorporating the use of Grade 690 MPa steel as reinforcement along with Grade 84 MPa concrete. A combination of wide flange bearing plate and flange doubler plate joint detailing was developed to improve the bearing and shear capacity of the joint. Also, a design methodology based on moment–curvature analysis was proposed to include the contribution of locked longitudinal reinforcement to bearing resistance. Subsequently, two large-scale interior beam-column subassemblies were subjected to quasi-static cyclic loading to verify the seismic behaviour of the proposed joint. One specimen was designed explicitly considering the material hardening and overstrength of steel beams. While the other was designed following the Taiwanese practice, which does not explicitly consider material hardening and overstrength but implicitly does it through strength reduction factors. Both the specimens exhibited a drift capacity of 4% with a stable and ductile hysteretic response and eventually failed through beam plastic hinging.

1. Introduction

Reinforced concrete column and steel beam (RCS) structural system is a composite moment-resisting frame with reinforced concrete (RC) columns and steel (S) beams. RC columns are economical, and their relatively higher stiffness makes them an attractive alternative compared to steel columns [1,2]. Similarly, steel beams can span longer distances than RC beams due to their high strength-to-weight ratio and steel beams do not crack like concrete beams under service loads. This makes RCS systems preferable for moment frames with large spans, which is typical for office buildings.

However, in regions of high seismicity, the high axial load on lower story columns, when combined with seismic load demands, generally makes the size of RC columns massive, along with issues of reinforcement congestion. The use of high-strength materials can not only reduce the column size but also solve the issues related to reinforcement overcrowding. Thus, in the past decade, guidelines for the design of new high-strength reinforced concrete (New-RC) with concrete grade (f_c') up to 100 MPa, longitudinal reinforcement with specified yield stress (f_{yl}) up to 690 MPa, and transverse reinforcement with specified yield stress (f_{yt}) up to 790 MPa have been developed [3]. The New-RC structures are suitable for high-rise RC residential buildings, which typically have shorter spans than office buildings. Experimental studies have demonstrated that New-RC columns are suitable for use in regions of high seismicity [4–6]. However, when it comes to RCS systems, most of the tests conducted in the past were on RCS beam-column joint subassemblies with columns made of normal-strength concrete and reinforcement. Hence, to make RCS systems competitive and effective, it is imperative to investigate the behavior of RCS systems with modern high-strength materials and develop design guidelines to assist structural designers.

The key element in developing the RCS structural system is the design of the RCS beam-column joint since the rest elements (columns

* Corresponding author.
E-mail address: yuchenou@ntu.edu.tw (Y.-C. Ou).

https://doi.org/10.1016/j.engstruct.2023.116186
Received 18 January 2023; Received in revised form 19 March 2023; Accepted 18 April 2023
Available online 29 April 2023

Nomenclature

Notations

A_g	cross-sectional area of column
A_h	beam flange cross-sectional area lost due to drilled holes at a given section
A_{st}	nominal cross-sectional area of longitudinal rebar
b_f	beam flange breadth
b_{fdp}	flange doubler plate breadth
b_{w-fbp}	wide-flange bearing plate (W-FBP) breadth
C_{cn}	nominal compressive strength of concrete bearing zone
C_{pr}	material strain hardening factor
C_{ri}	nominal compression strength contribution of locked rebars towards bearing
D	maximum displacement of the hysteretic loop
D_L, D_s	outer diameter of large and small spiral, respectively
d_j	distance between the centers of the steel beam flanges
E	modulus of elasticity of steel
E_D	energy dissipation per cycle of hysteresis loop
F^+, F^-	force at Δ^+ and Δ^-, respectively
f'_c	specified concrete compressive strength
f'_{ca}	actual concrete compressive strength on the test day
f_{lb}	longitudinal reinforcement strength contribution to bearing resistance
f_{lbh}	stress developed in longitudinal reinforcement under design load
f_u	specified ultimate stress
f_{ua}	actual ultimate stress
f_y	specified yield stress
f_{ysp}	specified yield stress of web doubler plate
f_{yl}, f_{yt}	specified yield stress of longitudinal and transverse reinforcement, respectively
f_{yp}, f_{yfdp}	specified yield stress of W-FBP and FDP, respectively
f_{ybf}, f_{ybw}	specified yield stress of steel beam flange and web, respectively
h	depth of concrete column measured parallel to the beam
h_{ri}	lever arm between locked longitudinal reinforcement
K_{eff}	effective/secant stiffness defined as $(F^+ - F^-)/(\Delta^+ - \Delta^-)$
$K_{\text{sec}\_0.5}$	secant stiffness at 0.5% drift
L_b	beam span
M_{bcf}	probable moment in the beam at the column face considering beam hinging
M_{cal}	beam nominal plastic moment capacity considering actual material strength ($Z_p f_{ya}$)
M_n	beam nominal plastic moment capacity ($Z_p f_y$)
M_{n_AISC}	beam probable moment capacity as per AISC 341
M_{nc}	nominal moment capacity of column as per new-RC guideline
M_{pb}	probable moment at the column centerline due to beam as per AISC 341
M_{pr}	probable moment demand in the beam at the plastic hinge location
M_{test}	peak moment demand at beam plastic hinge location obtained from experiment
M_{vb}	vertical moment bearing strength
M_{vr}	vertical moment bearing strength contribution from locked longitudinal rebars
P_{test}	average of peak applied load from experiment
R_y	material yield overstrength factor
R_{ya}	Actual material overstrength factor (Table 2)
S_h	distance of beam plastic hinge location from the column face
T_{ri}	nominal tensile strength contribution of locked rebars towards bearing
t_{sp}	thickness of web doubler plate
t_{bf}, t_{bw}	thickness of steel beam flange and web respectively
t_{fdp}	thickness of flange doubler plate (FDP)
t_{w-fbp}	thickness of wide-flange bearing plate (W-FBP)
V_b	bearing shear capacity of the joint
V_p	shear force at the plastic hinge location [36]
V_{col}	shear demand in the column
V_{ic}	horizontal shear strength of the inner concrete strut
V_{in}	nominal strength of the inner panel (steel panel + concrete strut)
V_n	nominal strength of joint
V_{on}	Nominal strength of outer concrete panel
V_{sp}	shear yield capacity of steel panel (steel beam web + doubler plate)
V_{test}	average of peak joint shear from experiment
V_u	horizontal joint shear force demand
Z_p, Z_f, Z_w	plastic section modulus of steel beam, beam flange, and beam web respectively
β_{eq}	equivalent viscous damping ratio
β_{eq_1-4}	average equivalent viscous damping ratio between 1% and 4% drift.
ϕ	strength reduction factor
ϕ_b	strength reduction factor for concrete bearing
ϕ_c	strength reduction factor for concrete strut
ϕ_s	strength reduction factor for steel panel shear
Δ^+, Δ^-	peak positive and negative displacement, respectively of loop
ρ_g	longitudinal reinforcement ratio
ρ_s	volumetric ratio of transverse reinforcement

and beams) are the same as that of RC and steel structures. Also, the behaviour of the RCS joint is heavily dependent on the type of 'additional attachments' used to assist the RCS joint in transferring beam moment and shear to the column. Over the years, the influence of multiple 'additional attachments' in the form of face bearing plates (FBP), web doubler plates, steel columns, steel bands, headed studs, cover plates, vertical reinforcement attached to beam flanges, etc., on the behaviour of RCS joints have been researched. With regard to the development of RCS design guidelines, ASCE published guidelines for 'through-beam' type RCS joints for use in low to moderate seismic regions in 1994 [7]. The 1994 ASCE guideline was based on multiple studies on the behaviour of RCS beam-column sub-assemblies conducted in the US and Japan till that date [8–10]. 'Through-beam' type refers RCS joints where steel beam passes continuously through the RC column. The procedure for joint bearing and shear strength estimation, joint transverse reinforcement detailing requirements, and the column longitudinal rebar size limits were also presented. Later, experimental tests of RCS joints and frames designed based on the 1994 ASCE guidelines demonstrated that the guidelines can be extended to be used in high seismic regions [11–18] with minor modifications. Thus in 2015, a new ASCE pre-standard for the design of RCS systems was published, which can be also used for seismic applications too [19]. In the ASCE pre-standard, additional design methods were proposed to include the design of more 'additional attachments' like steel bands, transverse beams, headed studs, and vertical joint reinforcement. Moreover, refined joint bearing and shear strength estimation procedures were developed.

Further, designs for 'through-column' type of RCS joints, where the

RC column runs continuously through the joint, have also been developed [20–22]. As steel beams are connected to the face of the RC column in 'through-column' designs, complexities associated with the reinforcement detailing within the joints are simplified. More recently, Alizadeh et al. [23,24] developed special bearing plate details to enhance joint bearing strength. Further, improvised RCS joints with details like extended bearing plates, embedded steel profiles, and shear keys to improve joint behaviour have also been developed [25,26]. Furthermore, the progressive collapse response of bolted RCS joint was investigated by Tang et al. [27], and recommendations were provided to improve collapse resistance. Finally, research by Yang et al. [28] developed re-centering RCS joint detail, which could significantly reduce residual drift.

Although numerous studies on RCS joints have been performed, most of the studies considered RCS joints with normal-strength materials. For instance, the ASCE pre-standard [19] restricts the steel grade of longitudinal reinforcement to 410 MPa (f_{yl}=410 MPa). Thus in 2022, research by Ou et al. [29] combined New-RC columns (columns with high-strength reinforcement and concrete) with steel beams to form New-RCS frames. The study by Ou et al. [29] used SD550 (f_{yl}=550 MPa) deformed bars as longitudinal reinforcement and had a design concrete strength ($f_c^{'}$) of 70 MPa. Bi-directional through-beam type joints were developed with concentric and eccentric connection details.

Thus, in continuation of the study by Ou et al. [29], the current study developed New-RCS joints with RC columns having reinforcement of Grade 690 MPa (f_{yl},f_{yt}=690 MPa) and design concrete strength ($f_c^{'}$) of 84 MPa. To the best knowledge of the authors, this is the first study in the literature that has used steel reinforcement with yield stress in excess of 550 MPa for columns of RCS systems. New-RC columns are suitable for use in high-rise special moment frames, where the columns and beams are subjected to high force demands. This high force demand translates to high shear and bearing force demands at the beam-column joint. Conventional RCS joint details are inefficient to resist such high force demands. Hence, the current study developed an innovative RCS joint referred to hereafter as 'New-RCS Joint' since New-RC columns are used in RCS systems. The proposed New-RCS joint uses a combination of a novel wide-flange bearing plate (W-FBP) and flange doubler plates (FDP) as additional attachments that can effectively mobilize the concrete strut within the joint to provide enhanced joint shear capacity. The use of FDP also results in enhanced joint bearing capacity. Additionally, a novel detailing method (locking longitudinal reinforcement) was introduced to make the column longitudinal reinforcement also participate in the bearing resistance of the joint. Design recommendations are available in the literature to quantify the contribution of longitudinal reinforcement to the joint shear strength for RC beam-column joints [30]. However, no design procedures are available to quantify the contribution of longitudinal reinforcement towards joint bearing resistance. Hence, a design procedure was formulated to estimate the contribution of longitudinal reinforcement towards joint bearing resistance, provided the longitudinal reinforcement is locked as done in the current study.

Further, two large-scale New-RCS beam-column subassembly specimens were tested to evaluate the seismic performance of the proposed joints. One specimen, similar to American practice [31] was designed with due consideration given to material hardening and overstrength while performing capacity design of the New-RCS joint. While the other specimen was designed without explicitly considering material hardening and overstrength of steel beams. The latter is important from the Taiwanese perspective [32] and other design standards that do not explicitly consider material overstrength (e.g. Indian steel code, IS-800 [33]). Nevertheless, the strength reduction factors used while estimating joint strength implicitly account for the overstrength of steel beams [32,34,35]. Thus, the comparison of the experimental response of specimens will help to evaluate whether explicit consideration of material hardening and overstrength of steel beams while performing capacity design has a considerable impact on the performance of the New-RCS joint, provided strength reduction factors are used while estimating the joint capacity.

2. Specimen design and experimental setup

2.1. Proposed design details for New-RCS joint

The current study developed a bi-directional through-beam type New-RCS joint (see Fig. 1), which is an improvement to the classical RCS joints [19] with regard to enhanced bearing and shear resistance of the joint. Through-beam eliminates the need for stringent detailing (weld and access hole) requirements to be followed in seismic steel beam-to-column connections [31,36]. In the New-RCS joint developed, the continuous beam is in the transverse direction. While the test beam (or welded beam) is attached orthogonally to the continuous beam by complete joint penetration (CJP) welds, as shown in Fig. 1**a**. In the experimental study conducted, it was the welded beam to which cyclic loading was applied. Loading welded beam will simulate the critical condition to test the efficacy of the weld detail provided.

To the cross frame formed by the two orthogonal steel beams, 'wide-face bearing plates' (W-FBP) were attached to the steel beams at the beam-to-column interface by CJP welds. In the proposed design, W-FBPs which extend beyond the column flanges were used (see Fig. 1). Though, W-FBPs were tested in the past [7,11], the shape of the proposed W-FBP is a novelty. In the past W-FBPs tested were extended in width alone and were confined between the bounds of the inner faces of the beam flange. In contrast, in the proposed W-FBP, the extension of the W-FBP beyond the beam flange extends between the outer faces of the beam flange (see Fig. 1). This shape of the W-FBP provides a stiffer detail, as W-FBP is also attached to the 'flange doubler plate' (FDP) by CJP welds. 'Flange doubler plate' (FDP) is a cross-shaped plate (see Fig. 1**b**) which is attached to the flanges of the steel beam through fillet welding. FDP has the same width as W-FBP. Finally, in one of the proposed joint designs, to strengthen the joint against bearing, a 'rebar locking nut' locked the longitudinal column reinforcement passing through the beam flanges (see Fig. 1**b**). This rebar locking nut detail is also a novelty intended to make the longitudinal column reinforcement participate in bearing resistance.

2.2. Specimen design

Specimen design details and material properties of the two large-scale interior New-RCS beam-column sub-assemblies tested as part of this research are summarized in Tables 1 and 2. The two specimens tested were named 'IJB' and 'IJBHO'. 'IJ' in the specimen nomenclature stands for 'interior joint'. 'B' stands for the intended failure mode, which is through flexural hinging of the 'beam'. Finally, 'HO' stands for the explicit consideration of material 'hardening and overstrength' while estimating the joint force demands. Today, seismic design standards (e.g. AISC 341 [31]) explicitly consider material hardening and overstrength of steel beam sections while estimating joint force demand. However, there are also design standards (e.g. Taiwanese and Indian steel codes [32,33]), which does not explicitly consider material overstrength (R_y=ratio of expected to specified yield stress), and material hardening factor (C_{pr}). Although Taiwanese provisions do not explicitly consider material hardening and overstrength, strength reduction factors used ($\phi_s\,(=0.9)/\phi_c\,(=0.75)/\phi_b\,(=0.65)$=reduction factors for steel panel shear/concrete strut/concrete bearing) in Taiwanese provisions [32,34,35] are different compared to American standards [31,37,38]. In this study, specimen IJB, which was designed following the Taiwanese strength reduction factors will help verify whether the Taiwanese design provisions can guarantee satisfactory seismic behaviour. While specimen IJBHO was also designed following the Taiwanese strength reduction factors, due consideration was given to material hardening and overstrength of steel beams while estimating joint force

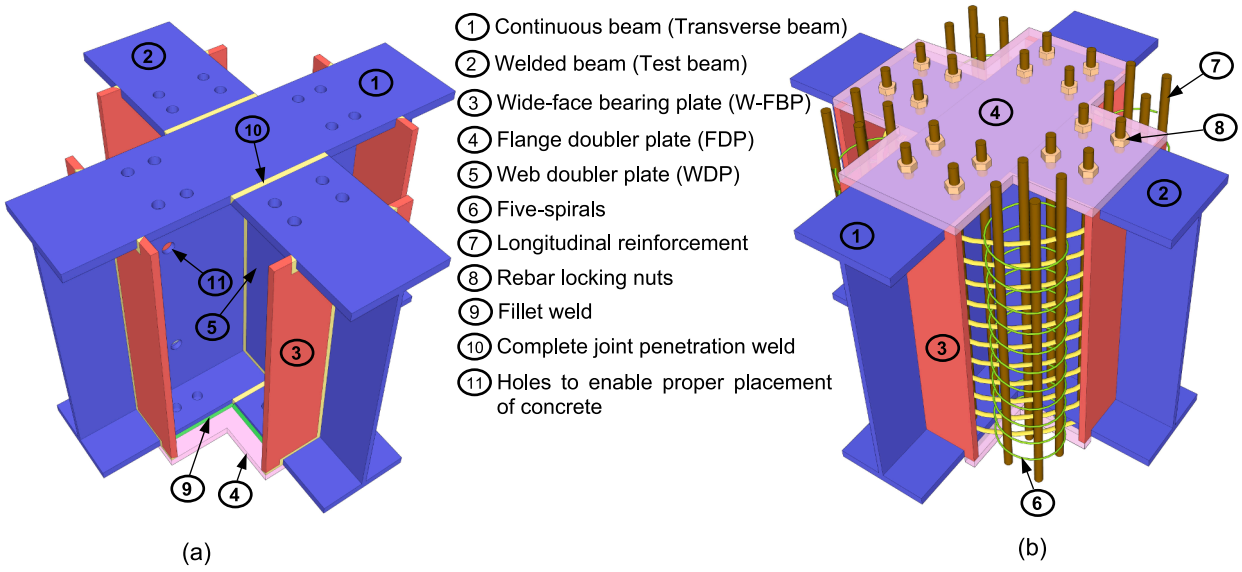

Fig. 1. Proposed joint design: a) steel framing of the joint with weld details before the attachment of flange doubler plate (FDP), and b) proposed joint.

Table 1
Design details of test specimens.

Specimen			IJB	IJBHO
Steel beam	Beam wide flange section (mm)		H900 × 300 × 16 × 28	H900 × 300 × 16 × 28
	Wide-Face bearing plate (W-FBP) (mm)		900 × 207 × 22	900 × 217 × 22
	Web doubler plate thickness t_w (mm)		–	14
	Flange doubler plate thickness t_r (mm)		28	30
	Flange doubler plate width (mm)		430	450
	Rebar hole diameter on beam flanges d_h (mm)		45	45
RC column	f'_c(MPa)		84	84
	f'_{ca}(MPa)		101	91
	Section (square) (mm)		800 × 800	800 × 800
	Height (mm)		4270	4270
	Longitudinal rebar		32 D36 (No. 11) SD690	32 D36 (No. 11) SD690
	Large spiral	Column	D16 (No. 5) @ 45 mm SD690, D_L = 740 mm	
		Joint	D16 (No. 5) @ 75 mm SD690, D_L = 740 mm	
	Small spiral	Column	D10 (No. 3) @ 45 mm SD690, Ds = 210 mm	
		Joint	D10 (No. 3) @ 75 mm SD690, Ds = 210 mm	
	Volumetric ratio of confinement reinforcement ρ_s (%)	Column	2.77	2.77
		Joint	1.66	1.66

D_L, D_S = *Outer diameter of large and small spiral, respectively.*

Table 2
Steel material properties of reinforcement and structural steel components.

	SD690 (D10)	SD690 (D16)	SD 690 (D32)	SN490B (steel beam flange)	SN490B (steel beam web)	SN490B (FDP)	SN490B (W-FBP)	SN490B (web doubler plate)
f_y(MPa)	690 (f_{yt})	690 (f_{yt})	690 (f_{yl})	330 (f_{ybf})	330 (f_{ybw})	330 (f_{yfdp})	330 (f_{yp})	330 (f_{ysp})
f_{ya}(MPa)	764	720	753	383	498	383	394	387
f_{ua}(MPa)	976	925	952	569	593	543	549	529
R_{ya} = f_{ya}/f_y	1.11	1.04	1.09	1.16	1.51	1.16	1.19	1.17

*Note: Considering beam flange (1.16) and web (1.51) material overstrength, for steel beam ($(Z_f f_{ya} + Z_w f_{ya})/Z_p f_y$ = 1.26).

demands. Thus, specimen IJBHO will help to evaluate whether consideration of material and hardening and overstrength on the top of Taiwanese strength reduction factors leads to considerable improvement in the seismic behaviour of the New-RCS joint.

In summary, as specimen IJBHO explicitly considered material overstrength and hardening, the force demand in the joint is higher compared to specimen IJB (Note: Both specimens use the same beam section). Thus, compared to specimen IJB, specimen IJBHO required wider W-FBP and FDP (see Table 1) to resist the increased force demand. Additionally, specimen IJBHO had web doubler plate and rebar locking nuts to increase the joint shear and bearing strength, respectively, which were not present in specimen IJB.

2.2.1. *Steel beam and concrete column design*

Built-up steel H section H900 × 300 × 16 × 28 mm with a span (L_b) of 7.56 m which is typical for beams in steel special moment frame

buildings were selected as the beams for both specimens (see Fig. 2). The beams used SN490B steel. RC columns with a square cross-section of 800 × 800 mm and a height of 4.27 m were designed following the New-RC design guidelines [3,39]. The concrete grade (f_c') was 84 MPa, and the steel reinforcement was SD690 (f_{yl}, f_{yt}=690 MPa). The actual compressive strength (f_{ca}') observed on the day of testing is listed in Table 1, and the actual steel rebar properties from the tensile test are mentioned in Table 2. RC columns had a longitudinal reinforcement ratio (ρ_g) of 5.03%. This column height and reinforcement ratio are typical for ground-storey columns in high-rise concrete frame buildings. As columns had a realistic longitudinal reinforcement ratio, the steel beam flanges had to be drilled to allow the passage of longitudinal reinforcement. Most of the experiments reported in the literature conveniently had rebars passing only through the corners, which is not realistic considering the force demands and optimum design of columns in real buildings located in high-seismic zones.

Due to enhanced confinement characteristics, economy, and ease of fabrication, five-spiral detailing was used for transverse reinforcement [40–42]. Large and small spirals had an outer diameter of 740 mm and 210 mm, respectively (see Fig. 2c). The amount of five-spiral transverse reinforcement in the column conformed with the confinement requirements of ACI 318 [37] and the confinement calculation procedure is outlined in Yin et al. [40,41]. Further, the shear strength of RC column was estimated using the modified discrete computational shear strength model [43]. The shear strength requirement controlled the design of five-spirals within the column. The selected RC column and steel beam section resulted in a column-to-beam strength ratio ($\sum M_{nc}/\sum M_{pb}$) of 1.21. The nominal column moment strength (M_{nc}) was estimated following the New-RC design draft [3]. And the probable moment at the column centerline due to beam hinging (M_{pb}) was estimated following AISC 341 [31] provisions. The provided column-to-beam strength ratio satisfied the requirement of AC1 318 [37] for concrete special moment frames (>1.2).

2.2.2. New-RCS joint design

2.2.2.1. Joint force demand. The joint shear demand (V_u) was estimated following **Eq. (1)**, which is the same as the one recommended by ASCE pre-standard [19].

$$V_u = \sum \frac{M_{bcf}}{d_j} - V_{col} \tag{1}$$

where, M_{bcf} is the beam bending moment at the column face considering beam plastic hinging, d_j is centerline distance between beam flanges, and V_{col} is the shear force in the column. For design purpose, the plastic hinge is assumed to be formed at the column face (S_h=0). M_{bcf} was estimated using **Eq. (2)**.

$$M_{bcf} = M_{pr}\ (M_{pr} = C_{pr}R_y f_y Z_p) + V_p S_h \tag{2}$$

where f_y and Z_p are the specified yield stress and plastic section modulus, respectively of steel beam, S_h is the distance of beam plastic hinge from column face, and V_p is the shear at the beam plastic hinge location [36]. As specimen IJB was designed following the Taiwanese code [32], which does not explicitly consider the material hardening factor (C_{pr}) and material overstrength factor (R_y); the probable moment capacity of the beam section (M_{pr}) was estimated by considering C_{pr} and R_y to be unity. While for specimen IJBHO, C_{pr} and R_y were taken as 1.2 and 1.1, respectively, in line with the AISC 341 [31] recommendations. Beam flanges had a R_y value of 1.16 (see Table 2), justifies the use of 1.1 as R_y factor in design. The estimated joint shear demand (V_u) for both specimens is reported in Table 3.

2.2.2.2. Joint capacity. The joint strength of the test specimens was estimated following the guidelines prescribed in the ASCE pre-standard [19]. However, as discussed in this section, appropriate modification of the ASCE pre-standard was made to incorporate the strength contribution from W-FBP, FDP, and rebar locking nuts. The design strength of the joint is the sum of the nominal resistance of the inner (V_{in}) and outer (V_{on}) panels, multiplied by respective strength reduction factors. Inner panel contribution (V_{in}) considers steel panel (V_{sp}) and inner concrete strut (V_{ic}) strengths. However, the inner panel contribution is capped by the bearing strength of the joint (V_b). As per the ASCE pre-standard [19], the width of the outer concrete panel of the specimens is zero due to the extended width of W-FBP. The outer concrete panel width that can be mobilized has been fully included in the inner concrete panel. Hence the outer concrete panel (V_{on}) does not contribute to the design strength in the proposed joint detail. Nevertheless, the extended width of the W-FBP increases inner panel width, which significantly enhances the overall joint strength. The joint inner panel (ϕV_{in}) design strength is estimated using **Eq. (3)**.

$$\phi V_{in} = \phi_s V_{sp} + \phi_c V_{ic} \le \phi_b V_b \tag{3}$$

where V_{sp} is the shear yield strength of steel panel (beam web + web doubler plate), and V_{ic} is shear strength of the inner concrete strut. Refer ASCE pre-standard [19] for the equations to estimate V_{sp} and V_{ic}. **Eq. (3)** is the same as the design equation suggested by the ASCE pre-standard [19], except for the use of Taiwanese code strength reduction factors (ϕ_s = 0.9, ϕ_c = 0.75, ϕ_b = 0.65). ASCE pre-standard considers different strength reduction factors (ϕ_s = 0.85, ϕ_c = 0.85, ϕ_b = 0.75). The extended width of W-FBP significantly increases the strength contribution from the inner concrete strut. For instance, while the width of the beam flange (b_f) is 300 mm, the width of W-FBP (b_{w-fdp}) is 430 mm and

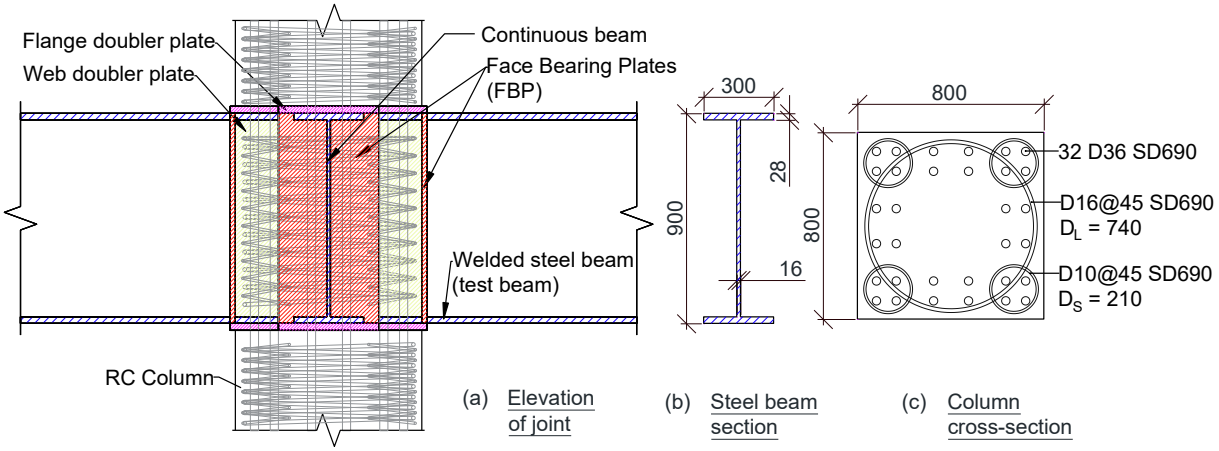

Fig. 2. A) elevation of proposed new-rcs joint, b) h-beam cross-section, and c) rc column cross-section (unit: mm).

Table 3
Joint capacity and shear demand.

Specimen	V_u (kN)	V_{sp} (kN)	V_{ic} (kN)	V_{on} (kN)	ϕV_{in} (kN)	M_{vr} (kNm)	C_{cn} (kN)	ϕV_b (kN)	M_{vb} (kNm)	ϕV_n (kN)	$\frac{\phi V_n}{V_u}$
IJB	5942	2281	5360	0	6073	0	18,782	6968	10,142	6073	1.02
IJBHO	7844	4277	5609	0	8056	1815	19,656	8483	12,429	8056	1.03

450 mm in specimens IJB and IJBHO, respectively. This corresponds to a 43% and 50% increase in concrete inner strut capacity (V_{ic}) for specimen IJB and IJBHO, respectively, as per **Eq. (3)**.

Fig. 3 outlines the procedure proposed to estimate the design joint bearing strength, $\phi_b V_b$. The main difference between the procedure available in ASCE pre-standard and the proposed procedure (see Fig. 3) is in the estimation of concrete bearing strength (C_{cn}) and the procedure adopted to calculate the contribution of locked rebars towards moment bearing strength (M_{vr}). As FDPs are used in the proposed joint, the concrete bearing area has the width of FDP (b_{fdp}) instead of flange width (b_f). Thus, using FDP resulted in a 43% and 50% increase in concrete bearing strength (C_{cn}) for specimens IJB and IJBHO, respectively.

In the proposed specimen IJBHO, the column longitudinal reinforcement, which passes through the beam flange, was attached to the beam flange/FDP using rebar locking nuts. A design procedure (see Fig. 3**b**) based on moment–curvature analysis was devised to estimate the contribution of the locked longitudinal reinforcement towards joint bearing resistance. In the moment–curvature analysis, Razvi et al. [44] concrete model is used, as this is the concrete model based on which the design stress block for high-strength RC lineal elements was proposed in the New-RC guidelines [3]. Further, an elasto-plastic constitutive model was used for SD690 (f_{yl}=690 MPa) longitudinal bars, where the compressive stress was limited to 600 MPa (corresponding to a concrete strain of 0.003), while in tension, the rebars develop their full yield stress of 690 MPa. Again, this elasto-plastic constitutive model was also recommended by the New-RC guidelines [3].

Table 3 summarizes the joint strength calculations used for specimen design. It can be seen from Table 3 that the ratio of design strength to joint force demand ($\phi V_n/V_u$) for specimens IJB and IJBHO were 1.02 and 1.03, respectively. This ratio was kept close to 1.00 to critically evaluate whether the proposed design can exhibit a desirable seismic response where the beam plastic hinging is the failure mode.

2.2.2.3. Additional attachments and joint confinement.. The following sub-sections enumerate the procedure adopted for the design of W-FBP, FDP and joint confinement. Fig. 4 shows the joint details of both specimens.

Wide-Face Bearing Plate (W-FBP).

W-FBP was designed following the provisions of the ASCE pre-standard [19]. However, the design equation was modified to incorporate the design of face-bearing plates which are wider than the beam flange. The thickness (t_{w-fbp}) and width (b_{w-fbp}) of W-FBP was estimated considering **Eq. (4)** and **Eq. (5)**, respectively.

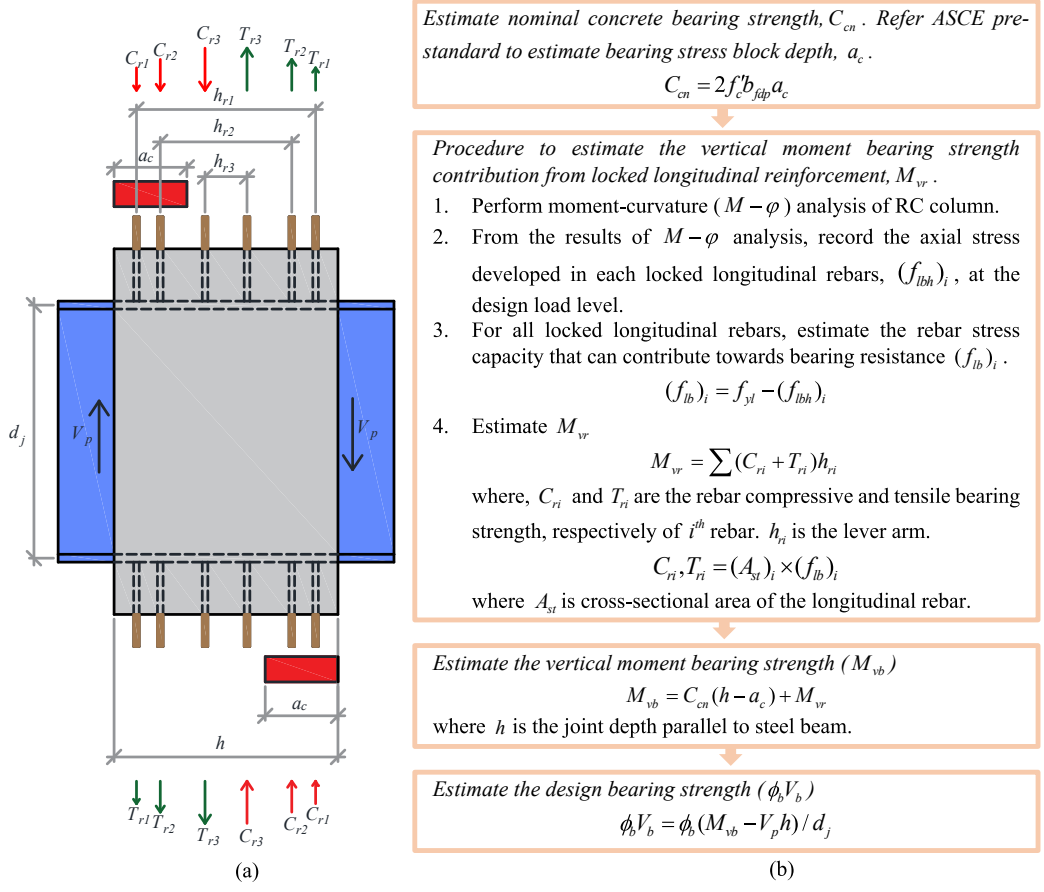

Fig. 3. A) free-body diagram of joint showing internal bearing forces in the vertical direction, and b) stepwise procedure to estimate joint bearing strength.

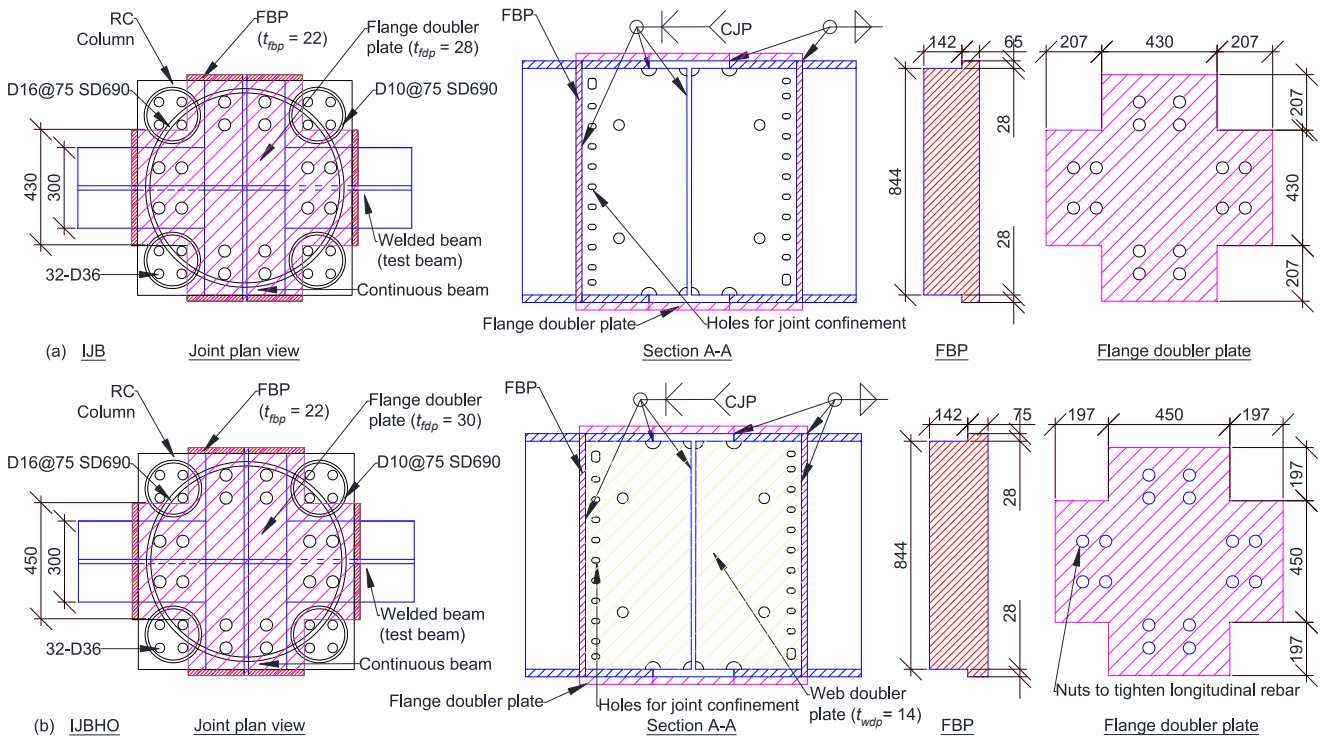

Fig. 4. Design details of joint: a) IJB, and b) IJBHO (Unit: mm).

$$t_{w-fbp} \geq \max\left(\underbrace{\frac{\sqrt{3}\,V_{ic}}{2b_{w-fbp}f_{up}}}_{\text{Limit shear stresses}} , \underbrace{0.20\sqrt{\frac{V_{ic}b_{w-fbp}}{f_{yp}d_w}}}_{\text{Limit bending stress}} , \underbrace{\frac{b_{w-fbp}}{22}}_{\text{For adequate section ductility}} \right) \tag{4}$$

$$b_{w-fbp} \leq 7t_{w-fbp} + b_f < 1.5b_f \tag{5}$$

where f_{yp} and f_{up} are the specified yield and ultimate strength of W-FBP. **Eq.** (4) is the same as the ASCE pre-standard provisions, except for the replacement of flange width (b_f) with the width of the W-FBP (b_{w-fbp}). **Eq.** (4) ensures that shear and flexural bending stresses due to interior concrete strut (V_{ic}) bearing against W-FBP do not lead to the shear failure or flexural yielding of W-FBP. **Eq.** (5) limits the bending flexibility of W-FBP. Due to the lack of experimental data, previous studies have arbitrarily limited the W-FBP width (b_{w-fbp}) to '$5t_{w-fbp} + b_f$' [8,9,11]. Considering the improvised W-FBP detailing (see *Section 2.1*) which results in a stiffer configuration, the maximum width of W-FBP is relaxed to '$7t_{w-fbp} + b_f$'.

Flange Doubler Plate (FDP).

Flange doubler plates (FDP) were added to stiffen the flanges of the steel beam within the joint, which were weakened by the holes drilled for column longitudinal reinforcement. The minimum thickness of FDP (t_{fdp}) is given by **Eq.** (6).

$$t_{fdp} \geq \max\left(\underbrace{1.2\frac{A_h}{b_f - \sum d_h}}_{\text{For reduction of beam flange}} , \underbrace{\frac{b_{fdp}}{0.64}\sqrt{\frac{R_y f_{yfdp}}{E}}}_{\text{For adequate section ductility}} \right) \tag{6}$$

where A_h is the beam flange cross-sectional area lost due to drilled holes at a given section, d_h is the diameter of drilled holes, f_{yfdp} is the specified yield stress of FDP, and E is the modulus of elasticity of steel. **Eq.** (6), developed by Ou et al. [29], ensures that the FDP thickness is sufficient to offset the loss of the beam flange due to drilled holes. Also, **Eq.** (6) ensures that FDP has adequate section-level ductility. FDP has the same width as W-FBP. Further, the beam flange thickness (t_{bf}) plus the FDP thickness (t_{fdp}) should be sufficient enough to resist a bearing force equal to the shear capacity of the steel panel, which can be checked by **Eq.** (7) [19].

$$t_{bf} + t_{fdp} \geq 0.3\sqrt{\frac{b_{fdp}(f_{ysp}t_{sp} + f_{ybw}t_{bw})d_j}{h(f_{ybf}t_{bf} + f_{yfdp}t_{fdp})/(t_{bf} + t_{fdp})}} \tag{7}$$

where f_{ybf}, f_{ybw}, f_{ysp}, and f_{yfdp} are the yield stresses of beam flange, beam web, web doubler plate and FDP, respectively, t_{bf}, t_{bw}, and t_{sp} are the thickness of beam flange, beam web, and web doubler plate, respectively.

Joint confinement.

Five-spiral reinforcement was used for joint confinement (see Fig. 4). The joint confinement satisfied the minimum volumetric ratio of joint confinement mandated by ACI-318 [37], and the confinement calculation procedure is outlined in Yin et al. [40,41]. The five-spiral spacing within the joint was 75 mm, while the five-spiral spacing within the column was 45 mm. This is because the confinement requirements governed the five-spiral spacing within the joint, while shear strength requirements governed the five-spiral spacing within the column.

2.3. Experimental setup and instrumentation

The experimental setup used in the current study is depicted in Fig. 5 which simulates an interior beam-column subassembly subjected to lateral load. The top end of the RC column was pin connected to four horizontal 100-tonne-force actuators that restrained the horizontal movement. The bottom end of the RC column was attached to a steel frame to simulate a pin connection. The RC column height between the top and bottom pin was 4270 mm. To stabilize the test setup, an axial compression of 0.05 $f'_{ca}A_g$ was applied and was maintained throughout testing.

Quasi-static displacement controlled cyclic loading was applied to the free ends of the test beams using two 100-tonne force actuators. Cyclic loading contained drift levels of 0.25%, 0.375%, 0.5%, 0.75%, 1%, 1.5%, 2%, 3%, and 4%. Loading to each drift level was repeated

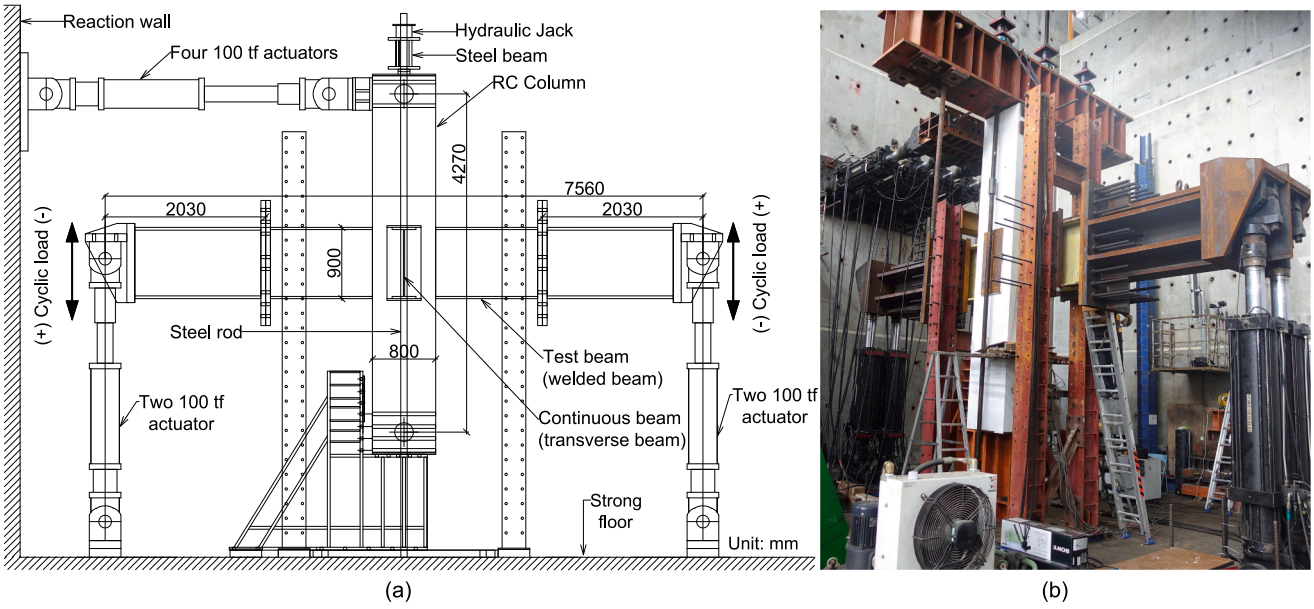

Fig. 5. A) experimental setup, and b) photo of experimental setup.

thrice. The chosen loading protocol adhered with the requirements of American Concrete Institute (ACI) guidelines for concrete moment resisting frames [45]. The drift level for interior beam-column joint specimens was determined by dividing the relative vertical displacement between beam ends by the beam span (7560 mm). To prevent premature lateral torsional buckling of steel beams, additional steel frames were provided to restrain out of plane movement. The applied forces and displacements of the actuators were recorded using load cells and LVDTs. Strain gauges were installed on the steel reinforcement, steel beam, and steel cross-frame within the joint to record the axial strain. In beam webs, strain rosettes were pasted to estimate the shear strains. The strain gauge location within the specimen is depicted in Fig. 6.

3. Test results and discussion

3.1. Crack patterns and failure mechanisms

At the end of cyclic loading, both specimens exhibited flexural plastic hinging of steel beams near the column face, while the joint was capacity protected as intended in the design. To begin with, at the start of the experiment, both specimens did not exhibit any signs of cracking after the axial load was applied, as the axial load level was only 0.05 $f'_{ca}A_g$. Thereafter, at 0.25% drift, minor horizontal flexural cracks induced by column moment appeared in the RC column, close to the beam flanges in both specimens. These cracks stabilized and did not grow considerably till the end of the test. At the first positive cycle of 1.0% drift, diagonal shear cracks began to appear in the joint of specimen IJB. This occurred almost simultaneously with the initiation of beam flange yielding in specimen IJB, as observed from the strain gauge readings. However, the diagonal shear cracks appeared at a later stage (1.50% drift) in specimen IJBHO. This delayed appearance of joint diagonal shear cracks was due to the design procedure adopted for specimen IJBHO where joint strength was increased by an additional web doubler plate, wider flange doubler and face bearing plates, and locking of selected column longitudinal reinforcement. In specimen IJBHO, the yielding of the beam flanges initiated at 1.0% drift which is the same as in specimen IJB. As the drift level increased, the yielding of the steel beam progressed at a faster pace compared to the expansion of diagonal shear cracks in both specimens.

The damage state of both the specimens at their corresponding peak sustained load is depicted in Fig. 7. At the first negative cycle of 3.0% drift, IJBHO reached its peak load. At the same time, specimen IJB attained its peak load at the first positive cycle of 4.0% drift. This is because, joint of specimen IJBHO had higher strength than specimen

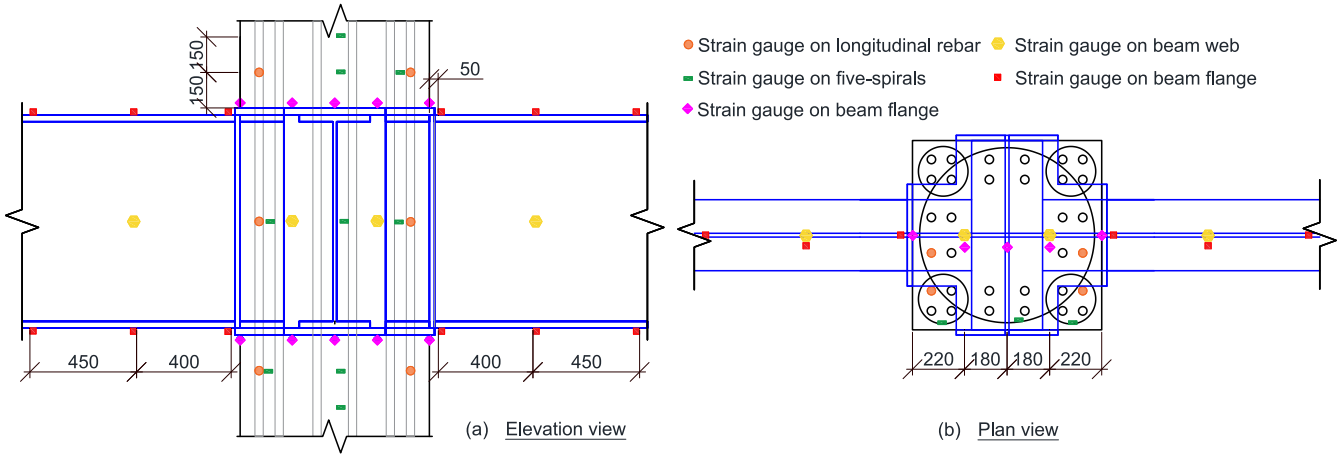

Fig. 6. Location of strain gauges: a) elevation view and b) plan view.

(a) IJB (+4.0% - first cycle) (b) IJBHO (-3.0% - first cycle)

Fig. 7. Damage condition of test specimens at their respective peak load: a) IJB, and b) IJBHO.

IJB. Hence, plastification of the steel beam progressed at a higher rate in specimen IJBHO compared to IJB. At the peak load, the extensive spalling of the paint in the beam flanges and minor spalling of the beam web (see Fig. 6) in both specimens clearly indicates inelasticity in the beam.

Finally, for both the specimens, the test was terminated at the last cycle of 4.0% drift, which is the minimum drift requirement recommended by American seismic provisions [31] for pre-qualification of beam-to-column connections of steel special moment frames. The testing could have been continued, but was terminated to examine the state of additional attachments, welds, and steel beam within the joint by dismantling the concrete in the joint region. At the end of 4.0% drift cycle, large local buckling of beam flange along with extensive yielding of the web was observed (see Fig. 8). It can be observed in Fig. 8 that, diagonal shear cracking of concrete in the joint is more extensive in specimen IJB compared to IJBHO while buckling of the beam flange is slightly more extensive in specimen IJBHO. Both observations are as expected from the design procedure adopted. The beam plastic hinge in both the specimens was located at a distance of approximately 0.3 d_j (d_j=depth of the joint) away from the column face. Furthermore, at the end of the test, no cracks in the bearing region of the column due to beam flange bearing on concrete was observed (see Fig. 8). Bearing cracks are typically vertical (or slightly inclined) cracks in the concrete column emanating from the edge of the beam flange. This indicates, that both the specimens had sufficient bearing strength, and the non-ductile bearing failure mode was averted.

Fig. 8**c** shows the steel frame of the joint post dismantling of joint concrete and reinforcement. It was observed that the W-FBPs, FDPs, web doubler plates, beam web and flanges inside the joint did not show any signs of buckling and performed as intended in the design. Also, all welds between joint elements remained intact. Further, the holes in the beam web to enable the placement of joint confinement did not lead to web plate tear or rupture. Finally, none of the joint confinement (five-spirals) provided fractured. Hence, the experimental testing confirms that the specimen designs achieved the desired seismic behaviour where the damage is primarily concentrated in the beam and the joint is capacity protected.

3.2. Hysteretic response of the specimens

The hysteretic response between the drift ratio and total applied load is depicted in Fig. 9. It can be seen that both specimens exhibited a stable and ductile hysteretic response, which is desired for seismic applications. Specimen IJB and IJBHO sustained a peak applied load of 1487 kN and 1497 kN, respectively (see Table 4). Both the specimens sustained very similar peak applied loads and had similar envelope response (see Fig. 9**c**) as the specimens had identical steel beams, which failed through flexural plastic hinging. Similar envelope response also means that the joints of both specimens had sufficient strength so that the difference in joint details did not significantly affect the hysteretic responses. A careful observation of the envelope response (see Fig. 9**c**) shows that specimen IJBHO had a slightly higher initial stiffness than IJB. This is expected as specimen IJBHO had a web doubler plate, wider W-FBP, wider FDP, and locked longitudinal rebars, all of which contributed to increased joint stiffness. To quantify the variation in stiffness, the change in secant stiffness with drift is presented in Fig. 10**b**. At a drift of

IJB (after the test) (b) IJBHO (after the test) (c) Joint steel frame

Fig. 8. Damaged state of specimens after the test: a) IJB, b) IJBHO, and c) joint steel frame.

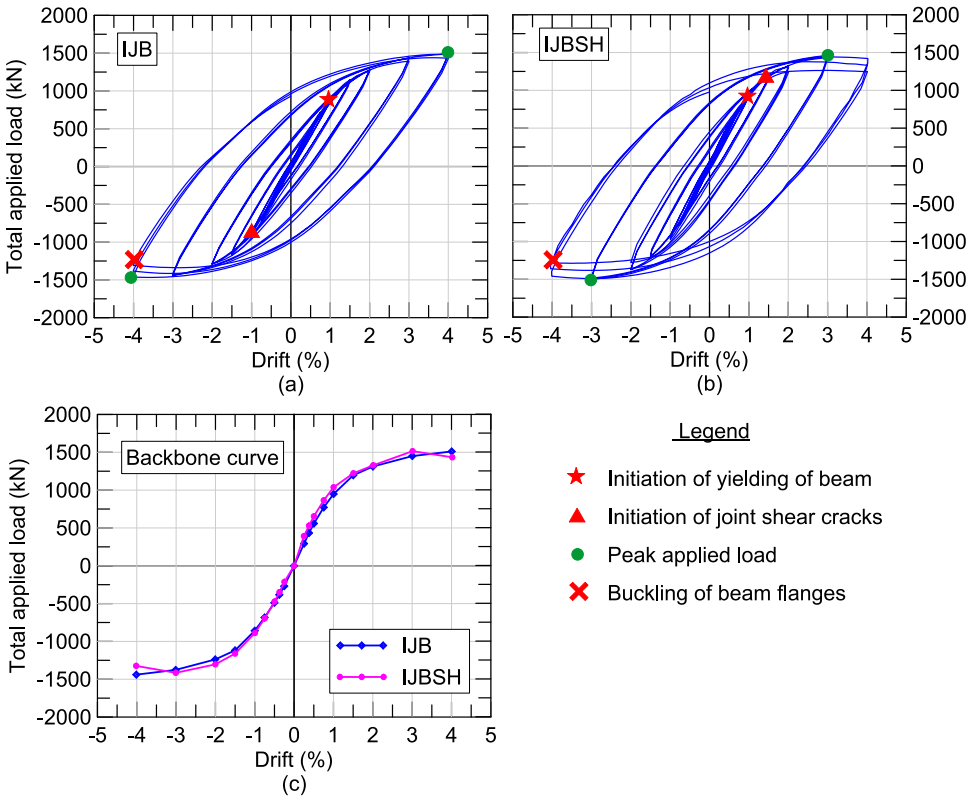

Fig. 9. Hysteretic response: a) IJB, b) IJBSH, and c) envelope response.

Table 4
Applied load, joint shear, average equivalent damping, and secant stiffness.

Specimen	Peak applied load					Joint shear demand			β_{eq_1-4} (%)	$K_{sec\_0.5}$ (kN/m)
	+		-		Average (P_{test})	+	-	Average (V_{test})		
	Drift (%)	Force (kN)	Drift (%)	Force (kN)	Force (kN)	Force (kN)	Force (kN)	Force (kN)		
IJB	4	1487	−4.01	1468	1478	8895	8781	8838	13.8	28,424
IJBHO	3.01	1462	−3.01	1497	1480	8745	8955	8850	16.4	30,714

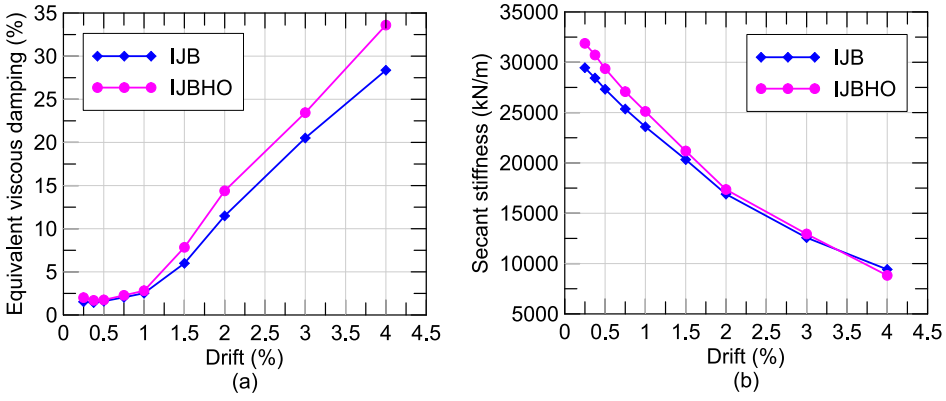

Fig. 10. A) equivalent damping, and) secant stiffness.

0.5%, specimen IJBHO exhibited an 8% increase in secant stiffness ($K_{sec\_0.5}$) compared to specimen IJB (see Table 3). However, by 2.0% drift, the variation of secant stiffness (K_{eff}) became less than 3%. This is because the specimen's stiffness began to be dominated by the steel beam, which was the same in both specimens. Eventually, at 4.0% drift, specimen IJBHO exhibited a 6% drop in secant stiffness compared to specimen IJB. This is because steel beam of specimen IJBHO exhibited larger local buckling (increased inelasticity) compared to specimen IJB. Finally, equivalent viscous damping, β_{eq} used to quantify energy dissipation was estimated using **Eq. (8)** [46].

$$\beta_{eq} = \frac{1}{2\pi} \times \left(\frac{E_D}{K_{eff} D^2} \right), \text{ where } K_{eff} = \frac{|F^+| + |F^-|}{|\Delta^+| + |\Delta^-|} \quad (8)$$

Fig. 10**a** depicts the variation of equivalent viscous damping with drift. Table 3 also shows specimens' average equivalent viscous damping between 1% and 4% drift (β_{eq_1-4}). It can be observed that specimen IJBHO exhibited a 19% increase in the average equivalent viscous damping (β_{eq_1-4}) compared to specimen IJB. This is because the energy dissipation of specimen IJBHO is contributed mainly by steel beam yielding and panel zone web yielding, both of which are highly ductile and stable means of energy dissipation. In the case of specimen IJB, the contribution of diagonal shear cracking to energy dissipation is higher in comparison to specimen IJBHO. Diagonal shear cracking is less ductile than steel beam yielding and panel zone web yielding. This explains the enhanced energy dissipation capacity of specimen IJBHO compared to IJB.

3.3. Strain responses

The strain response obtained from various locations of the test specimen is presented in Fig. 11. Due to the malfunction of strain gauges, strain measurements are missing in few plots. Fig. 11**a** shows the strain measurements from the strain gauge pasted on the steel beam flange near the column face. At 1% drift, flanges in both specimens began to yield. When specimens attained their corresponding peak applied load, the strain readings were above 0.01, indicating considerable strain hardening of the beam flange before flange local buckling. This observation points towards the need to incorporate the use of material hardening factor (C_{pr}) to reliably estimate the joint shear demands. Fig. 11**b** shows the shear strain measurements obtained from the strain gauges pasted on the beam web (within the joint) of specimen IJB. Reliable strain gauge reading was available till 0.75% drift only. The linearly increasing shear strain indicates that the beam web participated in shear resistance.

Fig. 11**c** shows the shear strain measurements obtained from the strain gauges pasted on the large spiral of the five-spiral joint confinement reinforcement provided. It can be observed that the large spirals remain elastic throughout the test providing effective confinement to the joint. This is because the proposed joint detail was effective in resisting

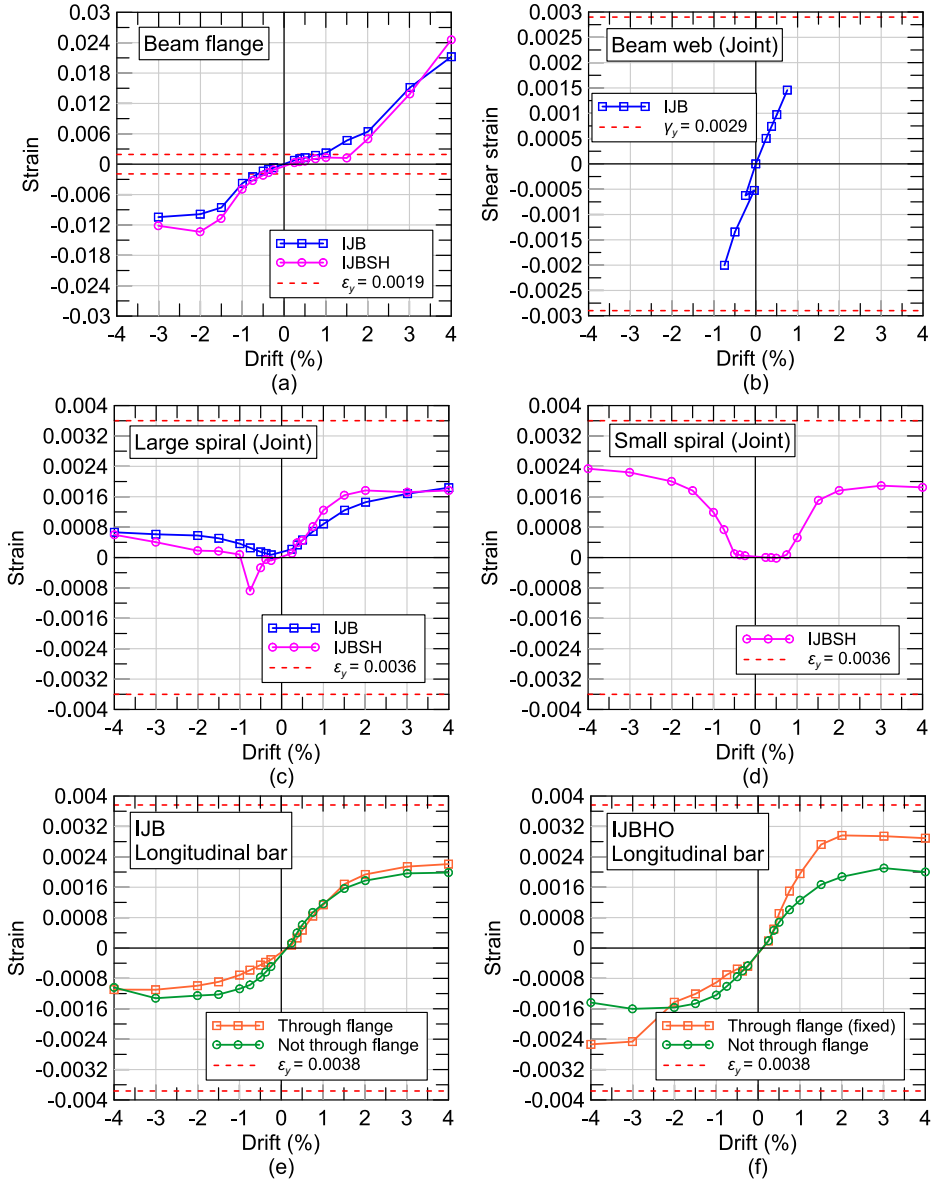

Fig. 11. Strain response envelope: a) steel beam flange close to column, b) steel beam web within the joint, c) large spiral within the joint, d) small spiral within the joint, e) column longitudinal reinforcement close to joint of specimen IJB, and f) column longitudinal reinforcement close to joint of specimen IJBHO.

the joint shear without significant diagonal cracking, which is desirable for seismic applications. Further, Fig. 11**d** shows the shear strain measurements obtained from the strain gauges pasted on the small spiral within the joint of specimen IJBHO. The small spiral also remains elastic throughout the course of loading. Thus, the elastic response of the five-spiral reinforcement indicates that the current ACI-318 [37] provisions are conservative in estimating the confinement requirement for the proposed New-RCS joint. This is because the proposed New-RCS joint had a transverse beam and was confined by W-FBP. The study by Ou et al. [29] has proposed a confinement reduction factor that can be applied for joint confinement reduction for RCS joints with transverse beams and face bearing plates.

Fig. 11**e and 11f** show the strain measurements from the column longitudinal reinforcement of specimen IJB and IJBHO, respectively. The strain gauges were pasted in the longitudinal reinforcement in the column close to the joint. All the longitudinal rebars remain elastic as intended in the design. In specimen IJB, strain readings of rebars not passing and passing through the beam flanges are nearly identical at all stages of the loading. In contrast, for specimen IJBHO, the column rebar passing through the flange developed a higher strain than the rebar not passing through the beam flange (see Fig. 10(**f**)). This implies that locking of rebars passing through the flanges in specimen IJBHO was effective in forcing the column rebars to also participate in bearing resistance. This observation validates the design procedure developed in the specimen design section (see Fig. 3**b**) to estimate the contribution of locked longitudinal rebars passing through the beam flanges towards bearing resistance.

4. Analytical prediction of experimental results

The analytically predicted capacity of the beam-column specimen subassemblies and corresponding experimentally obtained values are summarized in Table 5. The experimentally obtained capacity (M_{test}) of the specimen is the peak moment at the beam plastic hinge location. Specimen testing revealed that the beam plastic hinge formed at a distance of 0.3 d (d=beam depth) away from the column face. Thus, M_{test} is obtained by multiplying the average peak applied load (P_{test}) with the corresponding lever arm ($L_b/2-h/2-0.3d_j$). The beam's nominal moment capacity ($M_n = Z_p f_y$) was obtained by using the design material strength of the steel beam. The calculated capacity ($M_{cal} = Z_p f_{ya}$) of the beam corresponds to the plastic moment capacity estimated by considering the actual material strengths. Finally, the probable moment capacity ($M_{n\_AISC} = C_{pr} R_y Z_p f_y$) is estimated following the AISC 341 provisions [31]. The experiments show that the strain hardening factor (C_{pr}) was 1.09 (see Table 5) for both specimens, which is lower than the value suggested by AISC 341 ($C_{pr} = (f_u + f_y)/2f_y < 1.2$). Further, the steel beam's actual material overstrength factor (R_{ya}) was 1.26 (see Table 2), as observed from the tensile test of the steel beam flange and web coupons. This material overstrength value is higher than the 1.1 value considered in the design. Nevertheless, the AISC 341 provision was able to predict the moment capacity of the steel beam reliably, as the product of material overstrength and hardening ($R_y C_{pr} = 1.1 \times 1.2 = 1.32$) matched reasonably well with the experimentally observed values ($R_y C_{pr} = 1.26 \times 1.09 = 1.37$).

The experimentally observed moment capacities of specimen IJB and IJBHO were 4595 kNm and 4601 kNm, respectively. The moment capacities being very similar implies that the non-consideration of material hardening and overstrength by the Taiwanese steel design code [32] is offset by the conservative strength reduction factors of the Taiwanese code [32,34,35]. Further, both specimens satisfied the pre-qualification requirement of American seismic provisions [31] for beam-to-column moment connections. Thus, the experimental observations reveal that the explicit consideration of material hardening and overstrength on top of the current Taiwanese strength reduction factors is not required.

5. Conclusions

The design procedure and detailing for the New-RCS joint, which used high-strength steel reinforcement (Grade 690 MPa) and high-strength concrete ($f'_c = 84$ MPa), was developed, and its seismic behaviour was found to be satisfactory through large-scale experimental testing of two beam-column subassembly specimens. A combination of W-FBP, FDP, and rebar locking nuts was used as additional joint attachments to enhance joint strength. Based on the test results, the following conclusions and design recommendations are given:

1. Beam-column subassembly tests revealed that Grade 690 ($f_{yl} = 690$ MPa) column reinforcement did not hamper the seismic performance of the New-RCS joint developed in the current study. Hence, the maximum steel grade limit proposed by the ASCE pre-standard [19] to 410 MPa can be revised to include higher-grade steels up to 690 MPa. The New-RCS columns can be designed following the provisions of New-RC design guideline draft [3].
2. The combination of the proposed wide-flange bearing plate (W-FBP) and flange doubler plate (FDP) detail in the joint enhanced the concrete bearing and shear capacity in proportion to their extended width. The design guidelines for the W-FBP and FDP are described in the specimen design section.
3. The locking of column longitudinal reinforcement passing through the joint using nuts was effective in making the column longitudinal reinforcement also participate in joint bearing resistance. A design procedure based on moment–curvature analysis of the column cross-section to estimate the contribution of locked column longitudinal bars to bearing resistance was proposed. The design procedure is described in the specimen design section (see Fig. 3b).
4. The experimental tests revealed that both the test specimens had a drift capacity of 4%. Steel beams showed large flange local buckling along with extensive yielding of the web at the end of the 4% drift cycle. At the same time, the joints and columns were capacity protected as required for desirable seismic response. Thus, both specimens satisfied the pre-qualification requirement for beam-to-column moment connections of steel special moment frames recommended by American seismic provisions [31].
5. Specimen IJB, designed without the explicit consideration of steel beam material hardening and overstrength following the Taiwanese code, exhibited desirable seismic behaviour where the joint was capacity protected, and energy dissipation was primarily through beam plastic hinging. This is because the Taiwanese codes use conservative strength reduction factors while estimating joint strength. Hence, the explicit consideration of material hardening and overstrength on top of the current Taiwanese strength reduction factors is not required to design the proposed New-RCS joint. Specimen IJBHO, designed considering material overstrength and hardening along with Taiwanese strength reduction factors, also exhibited

Table 5
Comparison of experimental results and analytical predictions.

Specimen	M_{test} (kNm)	M_n (kNm)	M_{cal} (kNm)	M_{n_AISC} (kNm)	$C_{pr} = \frac{M_{test}}{M_{cal}}$	$R_y = \frac{M_{cal}}{M_n}$	$\frac{M_{test}}{M_{n\_aisc}}$
IJB	4595	3357	4224	4432	1.09	1.26	1.04
IJBHO	4601	3357	4224	4432	1.09	1.26	1.04

desirable seismic behaviour. Compared to specimen IJB, specimen IJBHO exhibited relatively less shear cracking in the joint along with slightly increased plasticity in the beam due to the increased joint strength. The use of wider W-FBP, FDP, and locking of longitudinal reinforcement at the joint led to increased joint strength of specimen IJBHO compared to specimen IJB.

Data Availability Statement

Experimental data presented and codes used in the study are available from the corresponding author upon request.

CRediT authorship contribution statement

Yu-Chen Ou: Conceptualization, Methodology, Resources, Writing – review & editing, Supervision, Project administration, Funding acquisition. **Jones Joju:** Methodology, Software, Formal analysis, Data curation, Writing – original draft, Validation, Visualization. **Bo-Cheng Lai:** Methodology, Software, Formal analysis, Investigation, Data curation. **Jui-Chen Wang:** Conceptualization, Supervision, Project administration.

Declaration of Competing Interest

The authors declare that they have no known competing financial interests or personal relationships that could have appeared to influence the work reported in this paper.

Data availability

Data will be made available on request.

Acknowledgements

The authors are grateful to National Science and Technology Council (NSTC) of Taiwan under Contract No. 109-2221-E-002-003-MY3 for financial support, Ruentex Engineering & Construction Co., Ltd for financial support and specimen fabrication, and National Center for Research on Earthquake Engineering (NCREE) of Taiwan for experimental facilities.

References

[1] Griffis L. Some design considerations for composite-frame structures. AISC Eng J 1986;130:59–64.
[2] Griffis L. Composite frame construction. In: Dowling PJ, Bjorhovde R, Hard JE, editors. Constr. steel Des., London: CRC Press; 1992, p. 523–54. https://doi.org/10.1201/9781482296709.
[3] NCREE. Design Guideline for Building of High-Strength Reinforced Concrete Structures (Draft). Taipei 2019.
[4] Ou YC, Nguyen NVB. Stress Limit for Shear Reinforcement of High-Strength Columns. ACI Struct J 2022;119:131–41. https://doi.org/10.14359/51733002.
[5] Ou Y-C, Alrasyid H, Nguyen NVB. Minimum Shear Reinforcement for Columns with High-Strength Reinforcement and Concrete. J Struct Eng 2020;147:04020313. https://doi.org/10.1061/(ASCE)ST.1943-541X.0002854.
[6] Ou YC, Alrasyid H, Haber ZB, Lee HJ. Cyclic behavior of precast high-strength reinforced concrete columns. ACI Struct J 2015;112:839–50. https://doi.org/10.14359/51687911.
[7] J Struct Eng 1994;120:2330–57.
[8] Sheikh TM. Moment connection between steel beams and concrete columns. University of Texas at Austin 1987.
[9] Deierlein GG. Design of moment connections for composite framed structures. University of Texas at Austin 1988.
[10] Sakaguchi N. Strength and behaviour of frames composed of reinforced concrete columns and steel beams. Kyoto University, 1992.
[11] Strength Ryoichi K. deformation, and seismic resistance of joints between steel beams and reinforced concrete columns. Cornell University; 1993.
[12] Parra-Montesinos Gustavo, Wight JK. Seismic response of exterior RC column-to-steel beam connections. J Struct Eng 2000;126:1113–21.
[13] Bugeja MN, Bracci JM, Moore Jr WP. Seismic behaviour of composite RCS frame systems. J Struct Eng 2000;126:429–36.
[14] Nishiyama I, Kuramoto H, Sugihiro K, Itadani H. Bi-directional behavior of interior-, exterior-, and corner- joints of RCS system. 12th World Conf. Earthq. Eng., vol. Paper No., Auckland, New Zealand: 2000, p. 1911.
[15] Deierlein G, Noguchi H. Overview of U.S.-Japan research on the seismic design of composite reinforced concrete and steel moment frame structures. J Struct Eng 2004;130:361–7. https://doi.org/10.1061/ASCE0733-94452004130:2361.
[16] Liang X, Parra-Montesinos GJ. Seismic Behavior of Reinforced Concrete Column-Steel Beam Subassemblies and Frame Systems. J Struct Eng 2004;130:310–9. https://doi.org/10.1061/ASCE0733-94452004130:2310.
[17] Cheng CT, Chen CC. Seismic behavior of steel beam and reinforced concrete column connections. J Constr Steel Res 2005;61:587–606. https://doi.org/10.1016/j.jcsr.2004.09.003.
[18] Cordova PP, Deierlein GG. Validation of the seismic performance of composite RCS frames: Full-scale testing, analytical modeling, and seismic design. CA 2005.
[19] Kathuria D, Miyamoto International Inc., Yoshikawa H, Nishimoto S, Kawamoto S, Taisei Corporation, et al. Design of Composite RCS Special Moment Frames. California: 2015.
[20] Nguyen XH, Le DD, Nguyen Q-H. Static behavior of novel RCS through-column-type joint: Experimental and numerical study. Steel Compos Struct An Int J 2019;32:111–26.
[21] Li W, Ye H, Wang Q, Liu H, Ding T, Liu B. Experimental study on the seismic performance of demountable RCS joints. J Build Eng 2022;49. https://doi.org/10.1016/J.JOBE.2022.104082.
[22] Chen H, Guo ZX, Basha SH, Liu Y. Seismic behavior of RCS frame joints applied with high-strength bolts-end plate connection. J Build Eng 2023;63. https://doi.org/10.1016/J.JOBE.2022.105455.
[23] Alizadeh S, Attari NKA, Kazemi MT. The seismic performance of new detailing for RCS connections. J Constr Steel Res 2013;91:76–88. https://doi.org/10.1016/j.jcsr.2013.08.010.
[24] Alizadeh S, Attari NKA, Kazemi MT. Experimental investigation of RCS connections performance using self-consolidated concrete. J Constr Steel Res 2015;114:204–16. https://doi.org/10.1016/j.jcsr.2015.07.026.
[25] Nguyen XH, Nguyen QH, Le DD, Mirza O. Experimental Study on Seismic Performance of New RCS Connection. Structures 2017;9:53–62. https://doi.org/10.1016/J.ISTRUC.2016.09.006.
[26] Khaloo A, Bakhtiari Doost R. Seismic performance of precast RC column to steel beam connections with variable joint configurations. Eng Struct 2018;160:408–18. https://doi.org/10.1016/J.ENGSTRUCT.2018.01.039.
[27] Tang H, Deng X, Jia Y, Xiong J, Peng C. Study on the progressive collapse behavior of fully bolted RCS beam-to-column connections. Eng Struct 2019;199:109618. https://doi.org/10.1016/J.ENGSTRUCT.2019.109618.
[28] Yang Y, Yang P, Shu Y, Shen PW, Eatherton MR. Experimental study on seismic behavior of the self-centering RCS joint with replaceable buckling restrained dampers. Eng Struct 2022;261:114288. https://doi.org/10.1016/J.ENGSTRUCT.2022.114288.
[29] Ou YC, Nguyen NVB, Wang WR. Seismic shear behavior of new high-strength reinforced concrete column and steel beam (New RCS) joints. Eng Struct 2022;265:114497. https://doi.org/10.1016/J.ENGSTRUCT.2022.114497.
[30] Pauletta M, Di Marco C, Frappa G, Somma G, Pitacco I, Miani M, et al. Semi-empirical model for shear strength of RC interior beam-column joints subjected to cyclic loads. Eng Struct 2020;224. https://doi.org/10.1016/J.ENGSTRUCT.2020.111223.
[31] AISC 341. Seismic Provisions for Structural Steel Buildings Supersedes the Seismic Provisions for Structural Steel Buildings. Chicago, Illinois: American Institute of Steel Construction; 2016.
[32] CPAMI. Design and Technique Specifications of Steel Structures for Buildings. Taipei, Taiwan: Construction and Planning Agency of of the Interior; 2010.
[33] IS 800. General Construction In Steel - Code of Practice. New Delhi, India: Bureau of Indian Standards ; 2007.
[34] CPAMI. Design Specifications for Concrete Structures. Taipei, Taiwan: Construction and Planning Agency of of the Interior; 2017.
[35] CPAMI. Design specification and Commentary for Steel-Reinforced Concrete Structures. Taipei, Taiwan: Construction and Planning Agency of of the Interior; 2011.
[36] AISC 358. Prequalified Connections for Special and Intermediate Steel Moment Frames for Seismic Applications, including Supplement No. 1. Chicago, IL: American Institute of Steel Construction; 2016.
[37] ACI 318. Building Code (ACI 318-19) and Commentary on Building Code Requirements for Structural Concrete. Farmington Hills, MI: American Concrete Institute; 2019.
[38] AISC 360. Specification for Structural Steel Buildings. Chicago, IL: American Institute of Steel Construction; 2016.
[39] Ou YC, Tsai TC. Design of high-strength reinforced concrete columns. J Chinese Inst Civ Hydraul Eng 2018;30:223–9. https://doi.org/10.6652/JOCICHE.201809_30(3).0006.
[40] Yin SY-L, Wu T-L, Liu TC, Sheikh SA, Wang R. Interlocking Spiral Confinement for Rectangular Columns. Concr Int 2011;33:38–45.
[41] Yin SYL, Wang JC, Wang PH. Development of multi-spiral confinements in rectangular columns for construction automation. J Chinese Inst Eng 2012;35:309–20. https://doi.org/10.1080/02533839.2012.655528.
[42] Ou YC, Lau JVJ, Li JY, Havlásek P, Bittnar Z. Cyclic behavior of reinforced concrete columns with five-spiral reinforcement. J Build Eng 2022:61. https://doi.org/10.1016/J.JOBE.2022.105245.
[43] Ou YC, Li JY, Roh H. Shear strength of reinforced concrete columns with five-spiral reinforcement. Eng Struct 2021;233:111929. https://doi.org/10.1016/J.ENGSTRUCT.2021.111929.

[44] Saatcioglu M, Razvi SR. High-Strength Concrete Columns with Square Sections under Concentric Compression. J Struct Eng 1998;124:1438–47. https://doi.org/10.1061/(ASCE)0733-9445(1998)124:12(1438).

[45] ACI 374.1. Acceptance criteria for moment frames based on structural testing and commentary : an ACI standard. Farmington Hills, MI: American Concrete Institute; 2005.

[46] Chopra AK. Dynamics of Structures. 5th ed. London: Pearson Education Limited; 2019.